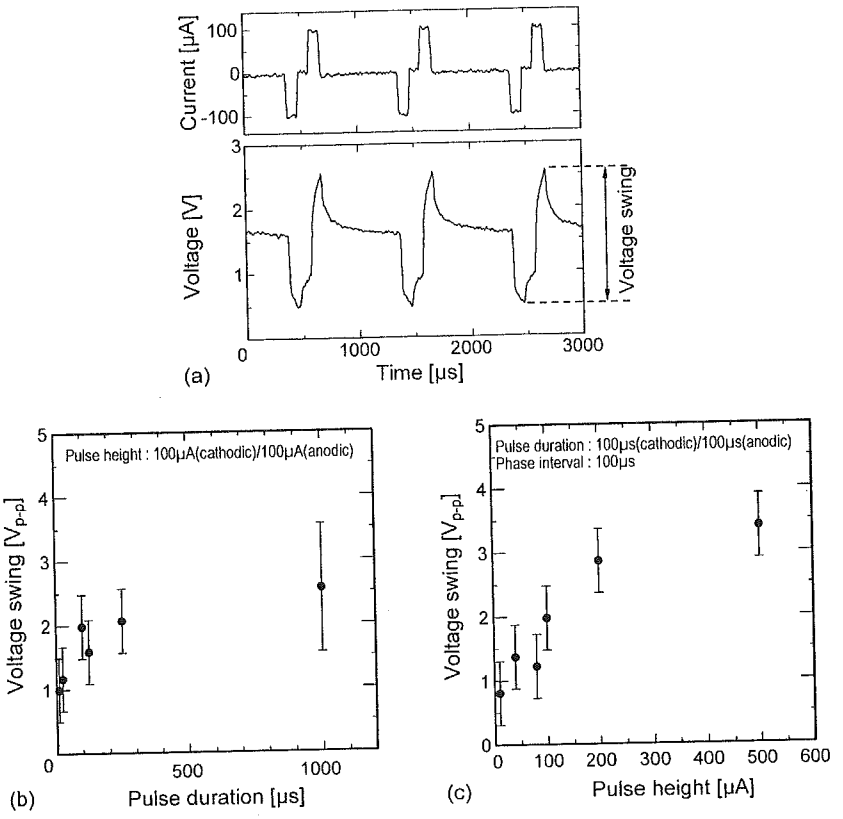

Fig. 10. (a) Typical voltage profile for current injection into a saline solution, and voltage swing as a function of (b) pulse duration and (c) pulse height.

[33,34]. The current injection for neural stimulation needs to be carried out without causing irreversible electrolysis or bubbles. The current injection capability depends on the material and surface structure of the electrode. In our experiments, no bubbles were observed on the Pt electrodes during the current injection, except for the condition of 100 μA (pulse height)/1000 μs (pulse duration). Thus, we can conclude that the present packaging with Pt/Au stacked bump electrodes is applicable for neural stimulation. The injection condition of 100 μA/1000 μs is beyond the capability of the present device with Pt/Au stacked bump electrodes because a small amount of bubbles were observed during the current injection.

Fig. 10(a) shows that the voltage settlement time required is several times longer than the durations of the current injection pulse, e.g. 300–500 μs for 100 μA/100 μs injection. On the other hand, the switching time of the device is shorter than 100 ns, as mentioned previously. The time required for address change in an incremental scan is negligible. Furthermore, we can even reset the device and re-select the electrode within 26 μs. This value means that we can scan the electrodes in random order at a cost of 26 μs/pixel or less. Most of the measurement time is spent for stimulation/recording. Although the device is not designed for multi-site simultaneous stimulation/recording, we believe that the device can be used as a high-speed, random-access neural interface device in the major part of 2D patterned neural stimulation/recording applications.

7. Conclusions

An LSI-based cooperative multi-chip neural interface device is proposed and designed. The proposed device consists of small (600 μm × 600 μm in the present design) intelligent neural interface chips (unit chips). The unit chips can be assembled with other unit chips and can work cooperatively. One can configure any number of the unit chips as a multi-chip neural interface device. The proposed multi-chip device is controlled via only four wires in its basic configuration. Compared to conventional single-chip architecture, the proposed multi-chip architecture has advantages of thinness, mechanical strength, flexibility, and extendibility. We have also developed packaging techniques for the cooperative multi-chip neural interface device. We demonstrated the fabrication of a thin, flexible packaging for small-sized multiple chips and LSI-compatible Pt/Au stacked biocompatible bump electrodes. The basic functions of the fabricated multi-chip neural interface device were characterized and the feasibility of the device as a random-access, multi-site stimulator was demonstrated.

Acknowledgements

This work was partly supported by the New Energy and Industrial Technology Development Organization (NEDO)

of Japan, and Health and Labor Sciences Research Grants, Japan.

References

[1] J. Chen, K.D. Wise, J.F. Hetke, S.C. Bledsoe Jr., A multichannel neural probe for selective chemical delivery at the cellular level, IEEE Trans. Biomed. Eng. 44 (1997) 760–769.

[2] Q. Bai, K.D. Wise, D.J. Anderson, A high-yield microassembly structure for three-dimensional microelectrode arrays, IEEE Trans. Biomed. Eng. 47 (2000) 281–289.

[3] M.O. Heuschkel, M. Fejtl, M. Raggenbass, D. Bertrand, P. Renaud, A three-dimensional multi-electrode array for multi-site stimulation and recording in acute brain slices, J. Neurosci. Meth. 114 (2002) 135–148.

[4] T. Kawano, Y. Kato, M. Futagawa, H. Takao, K. Sawada, M. Ishida, Fabrication and properties of ultrasmall Si wire arrays with circuits by vapor–liquid–solid growth, Sens. Actuators A 97/98 (2002) 709–715.

[5] E. Margalit, J.D. Weiland, R.E. Clatterbuck, G.Y. Fujii, M. Maia, M. Tameesh, G. Torres, S.A. D'Anna, S. Desai, D.V. Piyathaisere, A. Olivi, E. De Juan, M.S. Humayun, Visual and electrical evoked response recorded from subretinal electrodes implanted above the visual cortex in normal dogs under two methods of anesthesia, J. Neurosci. Meth. 123 (2003) 129–137.

[6] S. Takeuchi, T. Suzuki, K. Mabuchi, H. Fujita, 3D flexible multichannel neural probe array, J. Micromech. Microeng. 14 (2004) 104–108.

[7] T. Suzuki, D. Ziegler, K. Mabuchi, S. Takeuchi, Flexible neural probes with micro-fluidic channels for stable interface with the nervous system, in: Proceedings of the 26th International Conference on IEEE EMBS, San Francisco, CA, USA, September 1–5, 2004.

[8] L. Johnson, F.K. Perkins, T. O'Hearn, P. Skeath, C. Merritt, J. Frieble, S. Sadda, M. Humayun, D. Scribner, Electrical stimulation of isolated retinal with microwire glass electrodes, J. Neurosci. Meth. 137 (2004) 265–273.

[9] R. Rathnasingham, D.R. Kipke, S.C. Bledsoe Jr., J.D. McLaren, Characterization of implantable microfabricated fluid delivery devices, IEEE Trans. Biomed. Eng. 51 (2004) 138–145.

[10] R.J. Vetter, J.C. Williams, J.F. Hetke, E.A. Nunamaker, D.R. Kipke, Chronic neural recording using silicon-substrate microelectrode arrays implanted in cerebral cortex, IEEE Trans. Biomed. Eng. 51 (2004) 896–904.

[11] K. Najafi, K.D. Wise, An implantable multielectrode array with on-chip signal processing, IEEE J. Solid-State Circuits sc-21 (1986) 1035–1986.

[12] J. Ji, K. Najafi, K.D. Wise, A low-noise demultiplexing system for active multichannel microelectrode arrays, IEEE Trans. Biomed. Eng. 38 (1991) 75–81.

[13] S.J. Tanghe, K.D. Wise, A 16-channel CMOS neural stimulating array, IEEE J. Solid-State Circuits 27 (1992) 1819–1825.

[14] C. Kim, K.D. Wise, A 64-site multishank CMOS low-profile neural stimulating probe, IEEE J. Solid-State Circuits 31 (1996) 1230–1238.

[15] W. Liu, K. Vichienchom, M. Clements, S.C. DeMarco, C. Hughes, E. McGucken, M.S. Humayun, E. De Juan, J.D. Weiland, R. Greenberg, A neuro-stimulus chip with telemetry unit for retinal prosthetic device, IEEE J. Solid-State Circuits 35 (2000) 1487–1497.

[16] Q. Bai, K.D. Wise, Single-unit neural recording with active microelectrode arrays, IEEE Trans. Biomed. Eng. 48 (2001) 911–920.

[17] S.C. DeMarco, W. Liu, P.R. Singh, G. Lazzi, M.S. Humayun, J.D. Weiland, An arbitrary waveform stimulus circuit for visual prostheses using a low-area multibias DAC, IEEE J. Solid-State Circuits 38 (2003) 1679–1690.

[18] T. Kawano, Y. Kato, R. Tani, H. Takao, K. Sawada, M. Ishida, Selective vapor–liquid–solid epitaxial growth of micro-Si probe electrode arrays with on-chip MOSFETs on Si (1 1 1) substrates, IEEE Trans. Electron Devices 51 (2004) 415–420.

[19] Peter Fromherz, Neuroelectronic interfacing: semiconductor chips with ion channels, nerve cells, and brain, in: R. Waser (Ed.), Nanoelectronics and Information Technology, Wiley/VCH, Berlin, 2003, pp. 781–810.

[20] B. Eversmann, M. Jenkner, F. Hofmann, C. Paulus, R. Brederlow, B. Holzapfl, P. Fromherz, M. Merz, M. Brenner, M. Schreiter, R. Gabl, K. Plehnert, M. Steinhauser, G. Eckstein, D.S. Landsiedel, R. Thewes, A 128 × 128 CMOS bio-sensor array for extracellular recording of neural activity, IEEE J. Solid-State Circuits 38 (2003) 2306–2317.

[21] P.I. Pastor, I. Mody, J.W. Judy, In-vivo EEG recording using a wireless implantable neural transceiver, in: Proc. of the First International IEEE EMBS Conference on Neural Engineering, Capri Island, Italy, 2003, pp. 622–625.

[22] J. Ohta, N. Yoshida, K. Kagawa, M. Nunoshita, Proposal of application of pulsed vision chip for retinal prosthesis, J. Jpn. Appl. Phys. 41 (2002) 2322–2325.

[23] A. Uehara, K. Kagawa, T. Tokuda, J. Ohta, M. Nunoshita, Back-illuminated pulse-frequency-modulated photosensor using silicon-on-sapphire technology developed for use as epi-retinal prosthesis device, Electron. Lett. 39 (2003) 1102–1103.

[24] K. Kagawa, K. Isakari, T. Furumiya, A. Uehara, T. Tokuda, J. Ohta, M. Nunoshita, Pixel design of a pulsed CMOS image sensor for retinal prosthesis with digital photosensitivity control, Electron. Lett. 39 (2003) 419–420.

[25] D.C. Ng, K. Isakari, A. Uehara, K. Kagawa, T. Tokuda, J. Ohta, M. Nunoshita, A study of bending effect on pulsed frequency modulation based photosensor for retinal prosthesis, Jpn. J. Appl. Phys. 42 (2003) 7621–7624.

[26] K. Kagawa, K. Yasuoka, D.C. Ng, T. Furumiya, T. Tokuda, J. Ohta, M. Nunoshita, Pulse-domain digital image processing for vision chips employing low-voltage operation in deep-submicrometer technologies, IEEE J. Selected Top. Quant. Electron. 10 (2004) 816–828.

[27] A. Uehara, Y.-L. Pan, K. Kagawa, T. Tokuda, J. Ohta, M. Nunoshita, Micro-sized photo-detecting stimulator array for retinal prosthesis by distributed sensor network approach, Sens. Actuators A 120 (1) (2005) 78–87.

[28] J.D. Weiland, D.J. Anderson, Chronic neural stimulation with thin-film, oridium oxide electrodes, IEEE Trans. Biomed. Eng. 47 (2000) 911–918.

[29] S.F. Cogan, T.D. Plante, J. Ehrlich, Sputtered iridium oxide films (SIROFs) for low-impedance neural stimulation and recording electrodes, in: Proceedings of the 26th International Conference on IEEE EMBS, San Francisco, CA, USA, September 1–5, 2004.

[30] A.P. Chu, K. Morris, R.J. Greenberg, D.M. Zhou, Stimulus induced pH changes in retinal implants, in: Proceedings of the 26th International Conference on IEEE EMBS, San Francisco, CA, USA, September 1–5, 2004.

[31] A.J. Bard, R. Parsons, J. Jordan, Standard Potentials in Aqueous Solution, Marcel Dekker Inc., 1985.

[32] T.L. Rose, L.S. Robblee, Electrical stimulation with Pt electrodes. VIII. Electrochemically safe charge injection limits with 0.2 ms pulses, IEEE Trans. Biomed. Eng. 37 (1990) 1118–1120.

[33] S.B. Brummer, M.J. Turner, Electrical stimulation with Pt electrodes. II. Estimation of maximum surface redox (theoretical non-gassing) limits, IEEE Trans. Biomed. Eng. 24 (1977) 440–443.

[34] S.B. Brummer, M.J. Turner, Electrical stimulation with Pt electrodes. I. A method for determination of 'real' electrode areas, IEEE Trans. Biomed. Eng. 24 (1977) 436–439.

Biographies

Takashi Tokuda received his BS and MS degrees in electronic engineering from Kyoto University, Kyoto, Japan, in 1993 and 1995, respectively.

He received his Dr. Eng. degree in materials engineering from Kyoto University in 1998. He has been an assistant professor in the Graduate School of Materials Science, Nara Institute of Science and Technology, since 1999. He has been working on photonic materials science and photonic device engineering. He is a project member of the development of retinal prostheses devices. His research interests include CMOS image sensors, bio-imaging sensors, and bio-sensing devices. He is a member of the Japan Society of Applied Physics, and the Institute of Electronics, Information and Communication Engineers of Japan.

Yi-Li Pan received his BE in mechanical engineering from the National Sun Yat-Sen University, Taiwan in 1994. He obtained his BS in electronic engineering from the University of Warwick, UK in 2000. Currently he is a graduate student in the Graduate School of Materials Science of Nara Institute of Science and Technology, Japan. His research is focusing on the studies of retinal prosthesis.

Akihiro Uehara received his BS degree in electrical engineering from Osaka University, Japan in 1997, and MS degree from the Nara Institute of Science and Technology, Nara, Japan in 2000. In 2002 he joined the Nidek Vision Institute, Nidek Co. Ltd., Japan, where he has been engaged in the research of artificial vision prosthetic devices. His research interest is in CMOS sensors and mixed-signal circuit design.

Keiichiro Kagawa received his BE degree in applied physics from Osaka University, Japan in 1996. He received his ME and Dr. Eng. degrees in material and life science in 1998 and 2001, respectively. From 1995 to 2001, he was engaged in research on optical packaging and prototyping of optoelectronic parallel computers. Since 2001, he has been an assistant professor at the Nara Institute of Science and Technology, Nara, Japan. His research interests include CMOS image sensors, vision chips, and optoelectronic systems. He is a member of the Japan Society of Applied Physics, the Institute of Image Information and Television Engineers of Japan, and the Institute of Electrical and Electronics Engineers.

Masahiro Nunoshita was born in Okayama, Japan in 1942. He received his BE, ME and PhD degrees in electrical engineering, all from Osaka University, Japan, in 1965, 1967 and 1975, respectively. In 1967 he joined the Kyoto works, Mitsubishi Electric Corporation (MELCO), Japan. Since 1998 he has been a professor in the Graduate School of Materials Science, Nara Institute of Science and Technology, Nara, Japan. He is a member of the Japan Society of Applied Physics, the Institute of Electronics, Information and Communication Engineers of Japan, the American Physical Society, the Optical Society of America and the American Physical Society.

Jun Ohta was born in Gifu, Japan in 1958. He received his BE, ME, and Dr. Eng. degree in applied physics, all from the University of Tokyo, Japan, in 1981, 1983, and 1992, respectively. In 1983, he joined Mitsubishi Electric Corporation, Hyogo, Japan, where he has been engaged in the research on optoelectronic integrated circuits, optical neural networks, and artificial retina chips. From 1992 to 1993, he was a visiting researcher in Optoelectronics Computing Systems Center, University of Colorado at Boulder. In 1998, he has been an associate professor in the Graduate School of Materials Science, Nara Institute of Science and Technology (NAIST), Nara, Japan, and in 2004, he has been a professor of NAIST. His current research interests are in vision chips, CMOS image sensors, bio-photonic LSIs, integrated photonic devices. He received the Best Paper Award of the IEICE Japan in 1992, the Ichimura Award in 1996, and the National Commendation for Invention in 2001. He is a member of the Japan Society of Applied Physics, the Institute of Electronics, Information and Communication Engineers of Japan, the Institute of Image Information and Television Engineers of Japan, the Institute of Electronic and Electronics Engineers, and the Optical Society of America.

Available online at www.sciencedirect.com
SCIENCE DIRECT®
Biosensors and Bioelectronics 21 (2006) 1059–1068
BIOSENSORS & BIOELECTRONICS
www.elsevier.com/locate/bios

Functional verification of pulse frequency modulation-based image sensor for retinal prosthesis by in vitro electrophysiological experiments using frog retina

Tetsuo Furumiya, David C. Ng, Koutaro Yasuoka, Keiichiro Kagawa, Takashi Tokuda, Masahiro Nunoshita, Jun Ohta *

Graduate School of Material Science, Nara Institute of Science and Technology, 8916-5 Takayama, Ikoma, Nara 630-0101, Japan

Received 30 December 2004; received in revised form 5 April 2005; accepted 5 April 2005
Available online 10 May 2005

Abstract

The functioning of a 16 × 16 pixel pulse frequency modulation (PFM) image sensor for retinal prosthesis is verified through in vitro electrophysiological experiments using detached frog retinas. This image sensor is a prototype for demonstrating the application to in vitro electrophysiological experiments. Each pixel of the image sensor consists of a pulse generator (PFM photosensor), a stimulus circuit, and a stimulus electrode (Al bonding pad). The image sensor is fabricated using standard 0.6 μm CMOS technology. For in vitro electrophysiological experiments, a Pt/Au stacked electrode is formed on the Al bonding pad of each pixel and the entire sensor is fixed in epoxy resin. The PFM image sensor is confirmed experimentally to provide electrical stimulus to the retinal cells in a detached frog retina.

Keywords: Subretinal prosthesis; CMOS image sensor; Pulse frequency modulation; Packaging; In vitro electrophysiological experiment; Frog retina

1. Introduction

Retinal degenerative diseases such as retinitis pigmentosa (RP) and age-related macular degeneration (AMD) have resulted in various degrees of irreversible vision loss in tens of millions of people worldwide. Electrical stimulation of retinal cells by an implanted device has been reported to be an effective approach that allows partial recovery of visual sensation in blind patients. One such approach is to implant a subretinal prosthesis that replaces the function of damaged photoreceptor cells with optical-to-electrical converting devices (i.e. photosensors) in the subretinal space (Zrenner et al., 1997, 1999; Chow et al., 2001; Margalit et al., 2002; Zrenner, 2002). The subretinal prostheses reported to date are based on a micro photodiode array (MPDA) operating passively without a power supply in "solar cell" mode. Our group, however, has proposed an active device to provide more adequate stimulation of retinal cells (Ohta et al., 2002). Although an active device requires a power supply, it has the advantage that it can inject sufficient charge into the retinal cells and allows more effectively and adaptive control of the stimulus pulse parameters, such as height, width, and frequency. Other research groups working on subretinal prostheses have recently developed similar active photosensors (Ziegler et al., 2004; Zrenner, 2002).

In vitro and in vivo experiments are essential for the development of retinal prostheses, and such experiments have been carried out by many groups (Humayun et al., 1999; Grumet et al., 2000; Stett et al., 2000; Schanze et al., 2002; Humayun et al., 2003; Jensen et al., 2003; Li et al., 2005). These experiments, however, have been conducted for epiretinal prostheses. To the best of the authors' knowledge, there have been no reports on experiments involving active subretinal prostheses.

In general, epiretinal prostheses involve the implantation of a single planar electrode array in the epiretinal space (Humayun et al., 1994; Wyatt and Rizzo, 1996; Eckmiller, 1997; Margalit et al., 2002; Schanze et al., 2002; Deguchi et

* Corresponding author.
E-mail address: ohta@ms.naist.jp (J. Ohta).

0956-5663/$ – see front matter © 2005 Elsevier B.V. All rights reserved.
doi:10.1016/j.bios.2005.04.001

al., 2004). For subretinal prostheses, however, it is necessary to implant both a photosensor and an electrode array in the subretinal space.

We have proposed a pulse frequency modulation (PFM) photosensor with an integrated electrode as an active subretinal prosthesis (Ohta et al., 2002). The device is implanted between the retina and the retinal pigment epithelium (subretinal space). The PFM photosensor converts incident light into a digital pulse stream (Yang, 1994; Andoh et al., 2000). This pulse stream is suitable for direct stimulation of retinal cells. Other features of the PFM photosensor include robustness against noise, compatibility with logic circuits, wide dynamic range, and low-voltage operation, all of which are useful features for implanted devices. The characteristics of the PFM photosensors have subsequently been improve in order to stimulate retinal cells more effectively (Kagawa et al., 2003, 2004).

To apply this PFM photosensor in electrophysiological experiments, the sensor must be packaged in such as way to ensure biocompatibility, durability, and circuit protection. This packaging requirement also necessitates the integration of the stimulus electrodes with the PFM photosensor. The present report describes the fabrication of a 16×16 pixel PFM image sensor for use in in vitro electrophysiological experiments, and experimental verification of the prototype using detached frog retina.

This study is organized as follows. The fabrication, specifications and operation of the prototype prosthesis are presented in Section 2, and the packaging process and setup for in vitro experiments are described in Section 3. The ability of the PFM photosensor to stimulate retinal cells is confirmed through control the firing rate of retinal ganglion cell (RGC) spikes based on analysis of the dependence of the stimulus current amplitude and the frequency in the RGC response. Light-controlled stimulation using the PFM photosensor is also demonstrated. The experimental results are presented in Section 4 and discussed in Section 5, and the paper is finally summarized in Section 6.

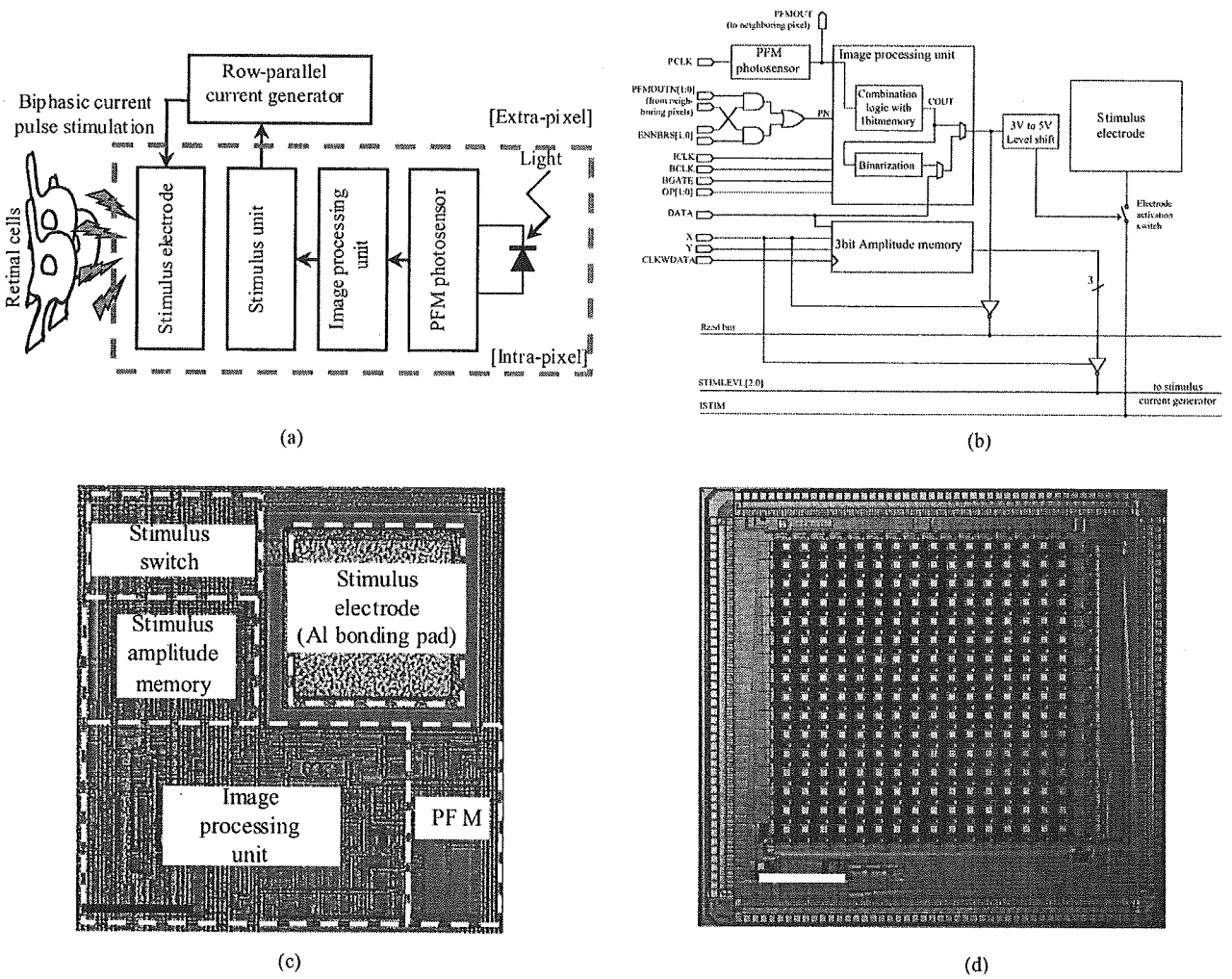

Fig. 1. (a) Block diagram of sensor architecture. (b) Simplified schematic. (c) Photomicrograph of image sensor pixel (scale bar: 80 μm). (d) Photomicrograph of image sensor (scale bar: 1 mm).

2. 16 x 16 pixel PFM image sensor for retinal prostheses

2.1. Sensor architecture and circuit design

Fig. 1a shows a block diagram of the sensor architecture. Incident light is converted into monophasic voltage pulses by a pulse generator, and the output is converted into biphasic current pulses by a stimulus unit and a row-parallel stimulus current generator. The biphasic current pulse stimulation is output from the stimulus electrode and forwarded to the retinal cells. This type of biphasic current pulse stimulation minimizes electrical damage to neural tissue and the electrodes and is thus desirable for neural cell stimulation (Lilly et al., 1955; Tehovnik, 1966; Barlett et al., 1977; Brummer and Turner, 1977; Margalit et al., 2002). A PFM photosensor was chosen for the generator as it produces a suitable pulse stream output and significantly simplifies downstream circuit, requiring only simple logic for signal processing.

A simplified schematic diagram and photomicrograph of a pixel are shown in Fig. 1b and c. Each pixel consists of a PFM photosensor, a processor unit, a 3 bit stimulus amplitude memory, a stimulus switch, and a stimulus electrode (Al bonding pad). Fig. 1d shows a photomicrograph of the fabricated 16 × 16 pixel PFM image sensor. The image sensor was fabricated using 0.6 μm 2-poly 3-metal standard complementary metal oxide semiconductor (CMOS) technology. The image sensor consists of a pixel array, a row-parallel stimulus current generator, and 4 bit X and Y decoders. The sensor consists of 16 × 16 pixels, with a pixel size of 240 μm × 240 μm. The number of pixels and pixel size were determined by the constraints of chip width (about 3 mm) and pixel separation (about 200 μm), as described previously (Kagawa et al., 2004). The supply voltages are 3 V for the logic circuits and 5 V for the stimulation circuit.

Each pixel consists of an N-well-P-substrate photodiode of 6 μm^2 in area and a 100 μm × 100 μm Al bonding pad as the stimulus electrode. The bonding pad is connected to the stimulus current circuits, which generate a biphasic current pulse with an amplitude range of −1 to +1 mA with 3 bit exponential and 3 bit linear resolution.

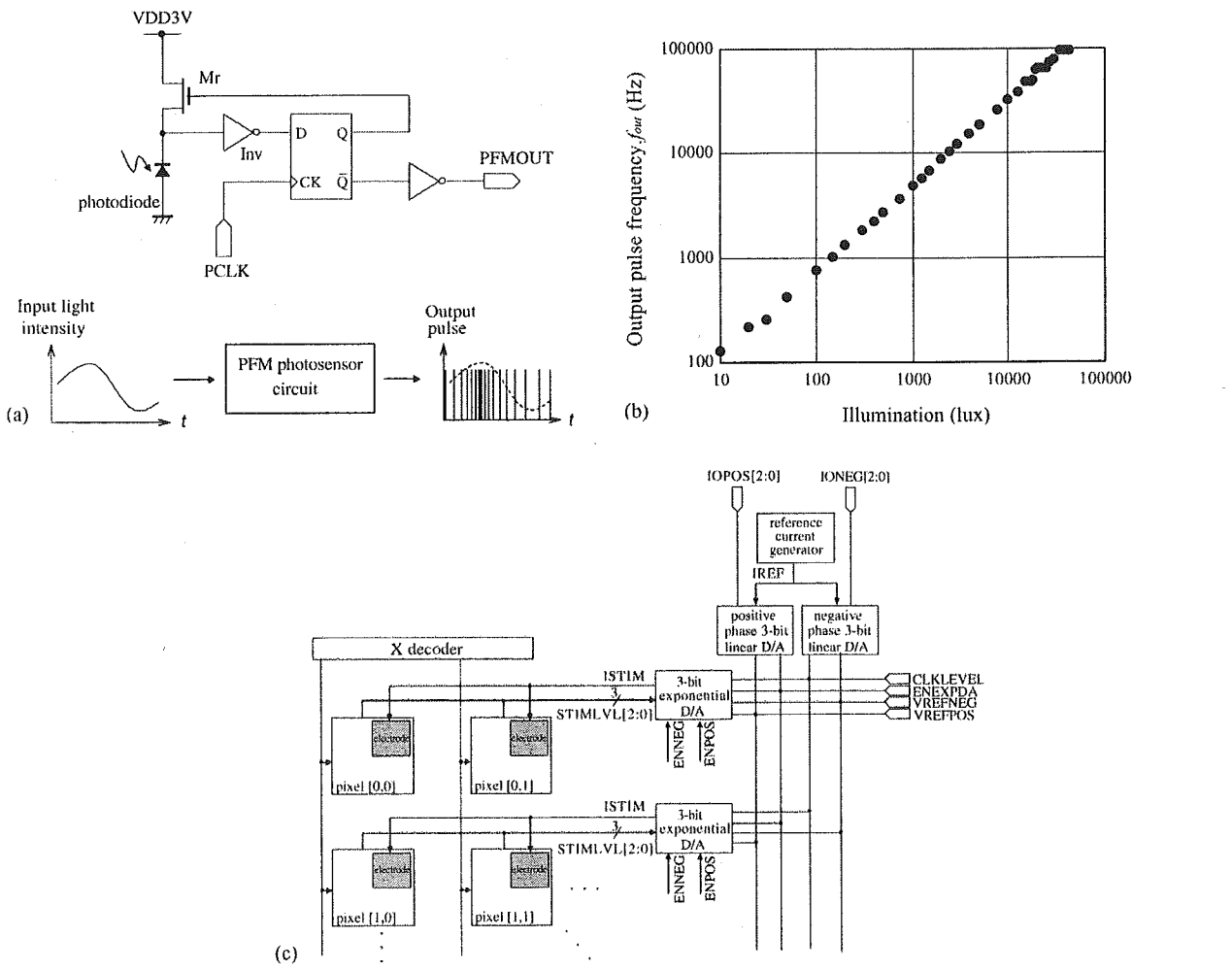

Fig. 2. (a) Schematic of PFM photosensor. (b) Experimental results showing the relationship between illumination intensity and output pulse frequency. (c) Simplified schematic of current generator block.

2.2. Photosensing

Photosensing is implemented using the PFM photosensor circuit. Essentially, the PFM circuit is a self-reset photodetecting circuit consisting of a comparator, a delay unit, and a reset switch, as shown in Fig. 2a. The comparator is implemented using an inverter (Inv), the threshold voltage of which is controlled by the supply voltage. A D-type flip-flop forces the output of the PFM circuit to be synchronized with the input clock (PCLK) and also delays the feedback signal, thus allowing sufficient time for resetting the photodiode. The reset signal controls the reset switch (Mr), which is an N-channel metal oxide semiconductor field effect transistor (MOSFET). As the reset signal is generated using the feedback of the output, the output frequency is a linear function of the input light intensity. The output pulse frequency (f_{out}) is approximated by

$$f_{out} = \frac{F}{1 + (F/f_{PCLK})}, \quad (1)$$

where $F = (i_L/C_{PD})(V_{DD} - V_{Trst} - V_{Tinv})^{-1}$, V_{Trst} and V_{Tinv} are the threshold voltages of Mr and Inv, and f_{PCLK} is the input clock frequency to the D flip-flop. From Eq. (1), the limiting value for f_{out} is F for very high input clock frequencies (f_{PCLK}). Introducing a power-correction parameter (γ) for the current versus illumination relationship, and assuming a unity denominator, f_{out} can be written as

$$f_{out} = \alpha L^{\gamma}, \quad (2)$$

where $\alpha = (Aq\eta/C_{PD})(V_{DD} - V_{Trst} - V_{Tinv})^{-1}$ is a constant describing the PFM circuit sensitivity, L is the illumination intensity, A is the effective photodiode area, q is the electron charge, and η is the quantum efficiency.

An example of the output of the PFM photosensor circuit is shown in Fig. 2b. An input signal of 1 MHz with a 50% duty cycle is used as the input clock (PCLK). The frequency of the output pulses is a linearly increasing function of light input intensity over a range of approximately four decades (~80 dB).

2.3. Stimulus current generation

A biphasic current pulse is used as electrical stimulus to the retinal nerve cells. The amplitudes of the positive and negative pulse are controlled using a 3 bit linear digital-to-analog converter (DAC) and a 3 bit exponential DAC. A schematic diagram of the current generator block is shown in Fig. 2c. The stimulus current amplitude level is first read from a preassigned 3 bit memory in each pixel. This is then used to set the exponential DAC driving current. Global 3 bit positive and negative phase currents (IOPOS[2:0], IONEG[2:0]) are used to tune the stimulus current to the desired value. The stimulus current amplitude I_{STIM} is given by

$$I_{STIM} = I_{REF} \times \frac{IO}{20} \times 2^{STIMLEVEL} \times 4, \quad (3)$$

where I_{REF} is the reference current, IO is the positive and negative linear DAC levels IOPOS and IONEG, and *STIMLEVEL* is the exponential DAC level.

3. Functional verification by in vitro electrophysiological experiment

To develop an effective retinal prosthesis, functional verification of the device through in vitro and in vivo experiments is necessary. To verify whether the device can actually stimulate retinal cells, it is necessary to test the device in electrophysiological experiments. Functional verification of the image sensor was performed in the present study by in vitro electrophysiological experiments using detached frog retina.

3.1. Packaging of the image sensor

The biological environment in which prosthetic image sensors are used presents some challenges. In applying the image sensor in electrophysiological experiments, it is important to consider biocompatibility, durability, and protection of the sensor. Most importantly, in the standard CMOS technology used to fabricate the image sensor, the surface of the image sensor is coated with SiO_x or SiN_x. While these coatings offer superior protection in air, they may degrade in biological environments. It is therefore necessary to protect the image sensor by fixing the device a biocompatible material. In addition, although only aluminum or copper is generally used for metallization in standard CMOS technologies, efficient stimulation of the retina cannot be achieved with such metals due to the lack of biocompatibility and low charge injection capability. Platinum is a suitable alternative that is widely used as a stimulus electrode in cochlear and retinal prostheses (Eckmiller, 1997; Humayun et al., 1999; Grumet et al., 2000; Schanze et al., 2002; Dormer, 2002).

The biocompatibility, durability, and protection requirements can therefore be satisfied by packaging the image sensor in a biocompatible material and employing Pt electrodes in a standard large-scale integration (LSI) chip. In the prototype presented here, a Pt/Au stacked electrode was fabricated on the stimulus electrode (Al bonding pad) of each pixel and the entire chip was fixed in epoxy resin, exposing only the stacked electrode. Fig. 3a and b shows a photomicrograph of the packaged chip. The Pt/Au stacked electrode was used due to its ease of fabricated on a standard LSI chip, for which a conventional ball bump bonder can be used, and its high durability compared to thin-film electrodes. Furthermore, the Au acts as a cushion for the Pt bump, where the direct formation of a Pt bump on the chip may damage the surface due to the hardness of Pt.

3.2. Retina preparation

Bullfrogs (*Rana catesbeiana*, 9–11 cm in length) were dark adapted for 30–45 min and the retina surgically re-

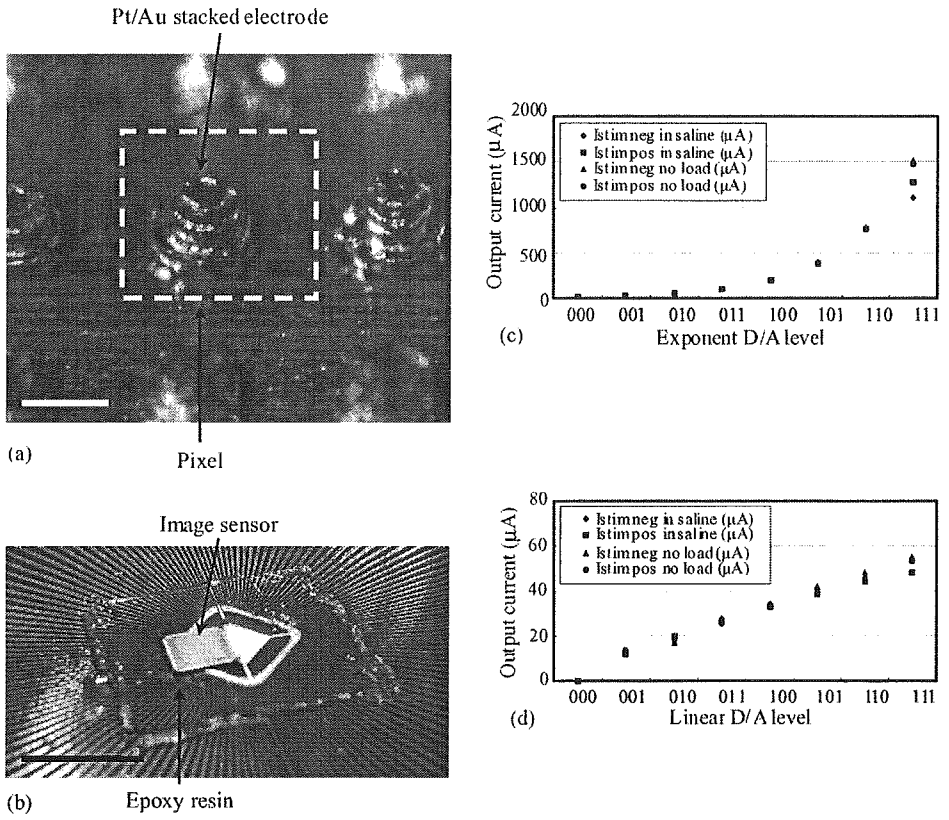

Fig. 3. Packaged image sensor showing: (a) Pt/Au stacked electrode on Al bonding pad (scale bar: 100 μm) and (b) epoxy resin protection layer (scale bar is 1 cm). Experimental results for operation in a biological environment: (c) exponential DAC, (positive and negative linear DAC parameters: IOPOS = 2, IONEG = 2), (d) linear DAC (common exponential DAC parameter: STIMLEVEL = 2). In these experiments, a negative-first biphasic current pulse train was used to output the current signal shape. Pulse parameters: negative pulse duration (D_n), 1 ms; positive pulse duration (D_p), 1 ms; inter-pulse duration (D_i), 1 ms.

moved under dim illumination. The eyeball was enucleated and hemisected. After the cornea and lens were removed, the sclera was separated from the pigment epithelium. The retina was then isolated from the pigment epithelium. A piece of retina about 3–5 mm wide was cut from the central part of the retina, and the piece of retina was positioned (RGC side up) on the surface of the packaged image sensor. Fig. 4a and b show the experimental setup. The retina was rinsed in a chamber with a ringer solution, then after removal of the ringer was fixed using a piece of ring-shaped filter paper. The ringer solution consisted of (in mM) NaCl 100, KCl 3.3, $CaCl_2$ 2, $MgCl_2$ 1, Glucose 10, and HEPES 10.

3.3. Stimuli

Experiments were carried out under microscope observation with infrared (IR) sensitive optics (LMPlan IR 5× lens, Olympus). Images were captured using an IR charge-coupled device (CCD) camera (MC-781R-0030, Texas Instruments), and adjusted in real time by an image processing unit (XL-20, Olympus). To confirm the condition of the retinal cells and the position of the recording electrode, light stimulation was performed at the start of the experiment. For this stimulation, the retina was irradiated with full-field diffuse light from a green light-emitting diode (LED; RT1027GPT, Okaya Electric Industries; peak wavelength, 530 nm). A square-wave signal of 0.2 Hz with a 50% duty cycle was used to induce a response in the RGCs (Ishikane et al., 1999).

After recording the light-induced RGC response, electrical stimulation was performed using a single selected pixel of the image sensor. A tungsten stimulus reference electrode (UJ-3002A, Unique Medical; impedance, 1 MΩ; tip diameter, 5 μm) was placed on the retina to produce a transretinal current. The position of the tungsten electrode was controlled using a manipulator (NHW-3, Narishige). Fig. 4c shows the electrical stimulation signal. A negative-first biphasic current pulse train was applied. The stimulus current amplitude (positive, I_p; negative, I_n), negative pulse duration (D_n), inter-pulse duration (D_i), and positive pulse duration (D_p) were controlled by the image sensor. After electrical stimulation, light stimulation was performed again to confirm that the same initial stimulation response was obtained.

3.4. Recording

A silver electrode (impedance, 5 kΩ; tip diameter, 50 μm) was used to record the extracellular response of the RGCs. The position of the silver electrode was controlled using another manipulator (NHW-3, Narishige). The distance between the tungsten electrode and the silver electrode was set

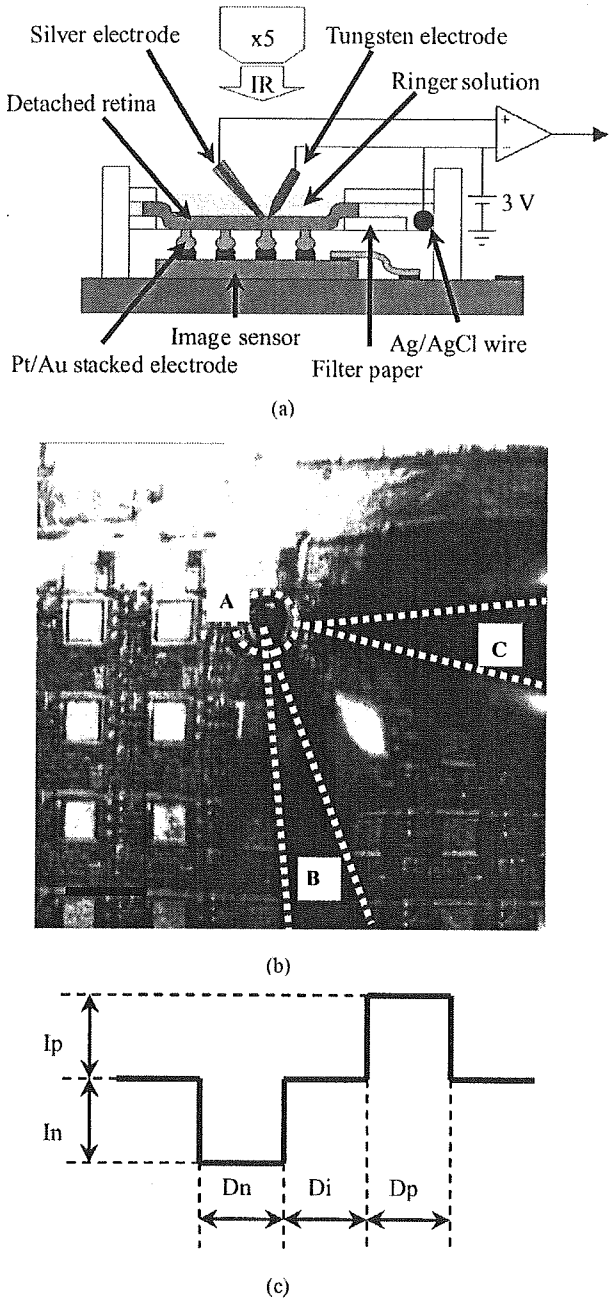

Fig. 4. Experimental setup showing: (a) side view of set-up and (b) microscopic top view of set-up. A tungsten electrode (B: stimulus reference electrode) is placed on a stimulus electrode (A: selected single pixel) through the retina. A silver electrode (C: recording electrode) is placed beside the tungsten electrode at a distance of 100 μm. (c) Diagram showing electrical stimulus waveform.

at about 100 μm. An Ag/AgCl wire was used as the reference electrode. The recorded response was amplified using an alternating current (AC) differential amplifier (DAM-80, World Precision Instruments; 0.3–10 kHz, 1000×). The amplified signal was sampled by a personal computer via an analog-to-digital converter (Micro 1401 mk II, Cambridge Electronic Design; 20 kHz, 16 bit).

The sampled data were analyzed using spike-detecting software (Spike2, Cambridge Electronic Design; discriminator mode). The sampled retinal cells response includes RGC responses (spike) and axon responses (spike). In extracellular recording, the response of the RGC is generally recorded as a biphasic spike, and the response of the axon is recorded as a triphasic spike. The axon exhibits two types of responses; one due to firing of the axon itself as a result of electrical stimulation, and one triggered by the connected RGC. As it is difficult to differentiate between these two axon responses, only the biphasic spike (RGC response) is analyzed.

4. Results

4.1. Operation in a biological environment

Fig. 3c and d shows the characteristics of the exponential and linear DACs. The stimuli currents for both the zero load and loaded cases were measured using the packaged image sensor and a current–voltage converter with a gain of 1000 V/A. A current output experiment in saline was also conducted to determine whether a packaged image sensor is suitable for in vitro electrophysiological experiments. These results show that the image sensor operates effectively in a biological environment and is capable of a positive/negative current output of 1 mA or more in saline. This current is sufficient for electrical stimulation of retinal cells.

4.2. Electrical stimulation

4.2.1. Dependence of response on stimulus current

The RGC responses obtained under electrical stimuli are shown in Fig. 5a. The induced activity was recorded at 24 locations on five retinas using a cathodic first biphasic current pulse train of $D_n = D_i = D_p = 1$ ms as the stimulus signal with current amplitudes of ±8, ±14, ±28, ±54 and ±106 μA. The stimulus timing was used as the external trigger signal. Stimuli were applied 20 times at each current amplitude at intervals of 5 s. The waveform that can be seen before the stimulus in the figure is an artifact due to noise from the input signals of the image sensor. Fig. 5b shows the induced RGC spikes at each stimulus current amplitude. A large peak within 30 ms and a small peak near 200 ms are observed. The large peak is believed to represent an enhancement response, while the small peak appears to be a suppression response or delayed response related to electrical stimulation. Fig. 5c shows the dependence of the firing rate on the stimulus current. These results indicate that the firing rate increases with stimulus current, thus demonstrating that the fabricated image sensor can successfully stimulate retinal cells.

4.2.2. Dependence of response on stimulus frequency

The RGC spikes induced by electrical stimuli at various frequencies are shown in Fig. 6a. The induced activity was

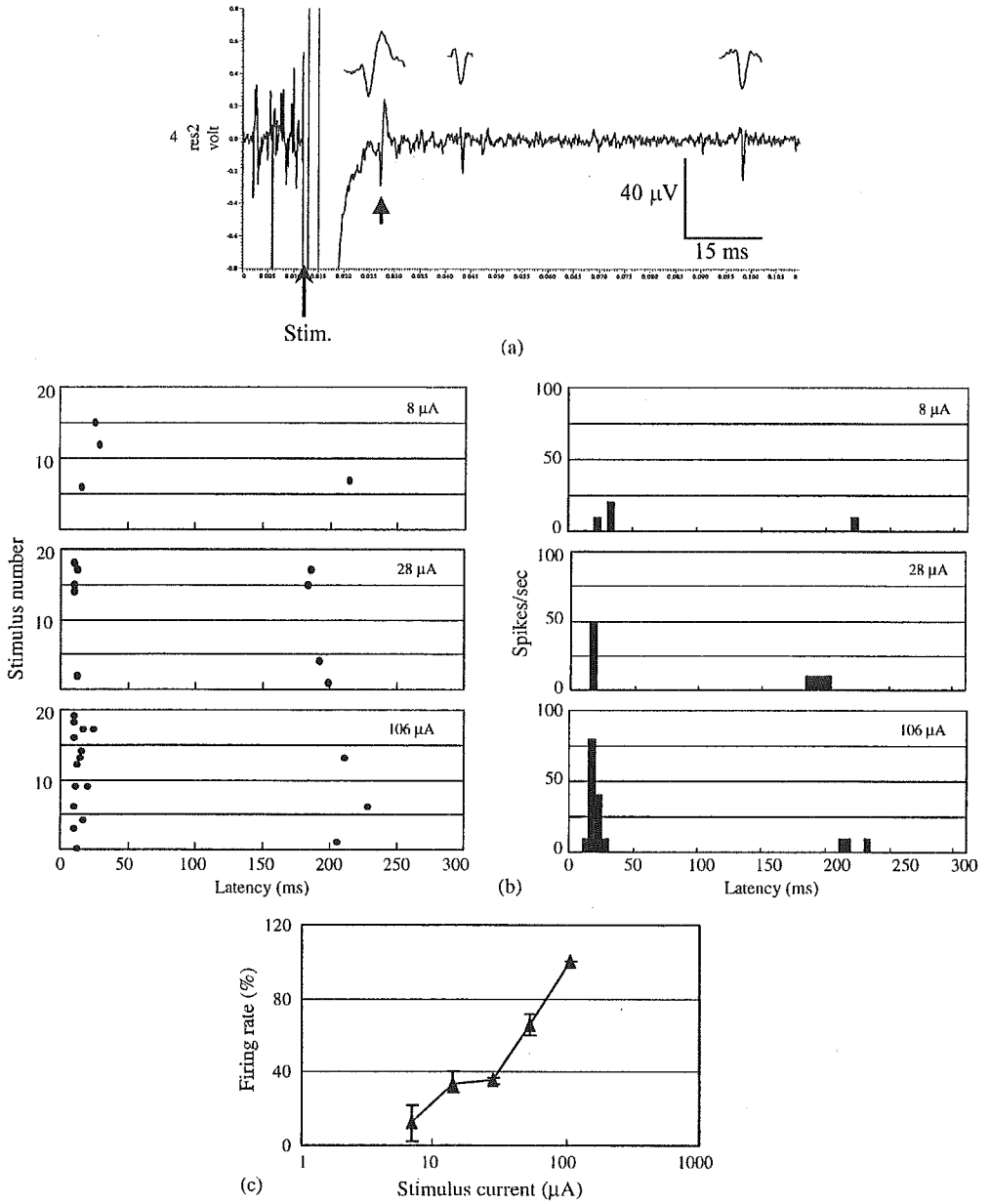

Fig. 5. Experimental results for stimulus current dependence of the response: (a) electrical stimulus-induced response of RGCs for Istim = ±28 μA and $D_n = D_p = D_i = 1$ ms. The biphasic spike is the RGC response (indicated by the arrowhead). The triphasic spikes are the axon response. Only the RGC spikes were analyzed. (b) Induced response related to strength of stimulus current amplitude, showing a raster plot (left) and histogram (right; bin width, 5 ms) of the RGC spikes at each stimulus current amplitude (20 stimuli). (c) Experimental results showing the relationship between the firing rate of the RGC spike and the stimulus current amplitude ($n = 3$).

recorded at 15 locations on five retinas using a cathodic first biphasic current pulse train of $D_n = D_i = D_p = 1$ ms at current amplitudes of ±28 and ±54 μA and stimuli frequency of 0.2, 1, 5 and 10 Hz. The stimulus timing was used as the external trigger signal. A total of 20 trials were performed for each stimulus frequency, and each trial lasted for 5 s, separated by an interval of 10 s (0 s at 0.2 Hz). Fig. 6b shows the dependence of the firing rate on the stimulus frequency. These results indicate that the firing rate increases with stimulus frequency. Thus, the firing rate can be controlled by the stimulus frequency.

4.2.3. Light-controlled stimulation

The RGC spikes induced by infrared light of various intensities are shown in Fig. 7a. The induced activity was measured at nine locations on three retinas using a cathodic first biphasic current pulse train of $D_n = D_i = D_p = 1$ ms with current amplitude of ±28 μA and frequencies of 0.2, 1 and 5 Hz (at 0.125, 0.625 and 3.125 lx; calculated from the photosensitivity of the image sensor). The stimulus timing and stimulus frequency were generated by the PFM photosensor. The sensor was irradiated with infrared light, for which the retina is insensitive, thereby ensuring that the measured response is

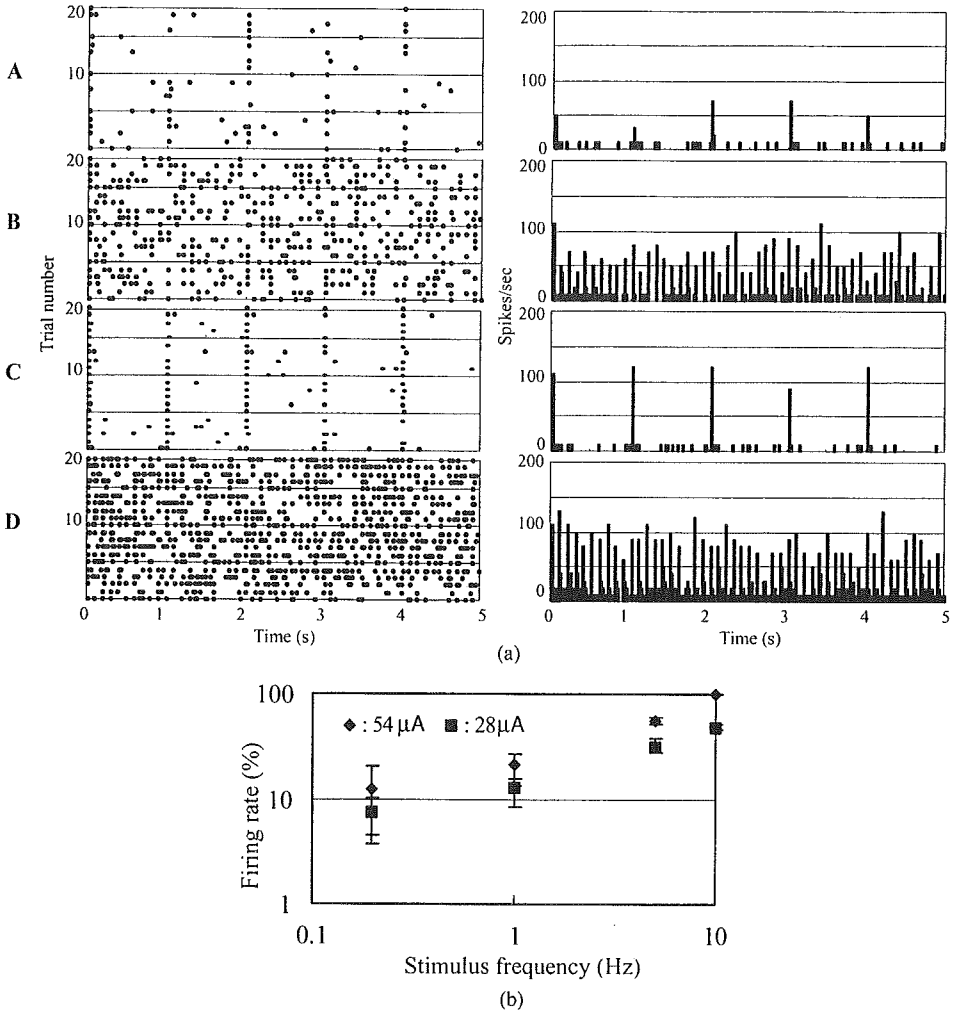

Fig. 6. Experimental results for stimulus frequency dependence of the response: (a) induced response related to frequency of stimulus signal, showing a raster plot (left) and histogram (right; bin width, 5 ms) of the RGC spikes at each stimulus frequency (20 trials). (A) 28 μA, 1 Hz; (B) 28 μA, 10 Hz; (C) 54 μA, 1 Hz; (D) 54 μA, 10 Hz. (b) Experimental results showing the relationship between the firing rate of the RGC spikes and stimulus frequency ($n = 3$).

due only to the stimulus signal generated by the image sensor. These trials were performed 20 times for each light intensity, with each trial lasting for 5 s and separated by an interval of 10 s (0 s for 0.2 Hz). Fig. 7b shows the relationship between the firing rate and the infrared light intensity. These results show that the firing rate increases with infrared light intensity and stimulus frequency. It can thus be concluded that the PFM photosensor can stimulate retinal cells in response to exposure to external light.

5. Discussion

A single prototype of the packaged image sensor was used in all 13 experiments (a total of 16.7 h) in the present study, and normally operation was observed throughout, indicating that the packaging technique is durable in a biological environment. In addition, the results for the stimulus current dependence are similar to the experimental results obtained for chicken retina implanted with a planar electrode array (Stett et al., 2000), supporting the functionality of the proposed sensor.

The stimulus frequency range adopted in the present experiments (0.2–10 Hz) is lower than the firing rate of spontaneous response. At higher frequencies, the sensor is susceptible to pronounced signal artifacting due to electrical stimuli and noise from the input signal of the image sensor. However, it has been reported that strong electrical stimuli induce 2–5 spikes in response to each event (Stett et al., 2000), suggesting that it is possible to induce a firing rate of about 50 Hz using a stimulus frequency of just 10 Hz. Further studies on this issue are therefore required.

In retinal prostheses, the spatial sensitivity distribution is an important parameter in visual sensation (phosphene), and can be recognized by a blind patient. This is also important in image reproduction. Although the spatial sensitivity distribution of the RGC response was not examined in the present study, several reports on the phenomenon have been published. In the case of chicken retina, the sensitivity radius has been determined to be 100–200 μm under charge injection of

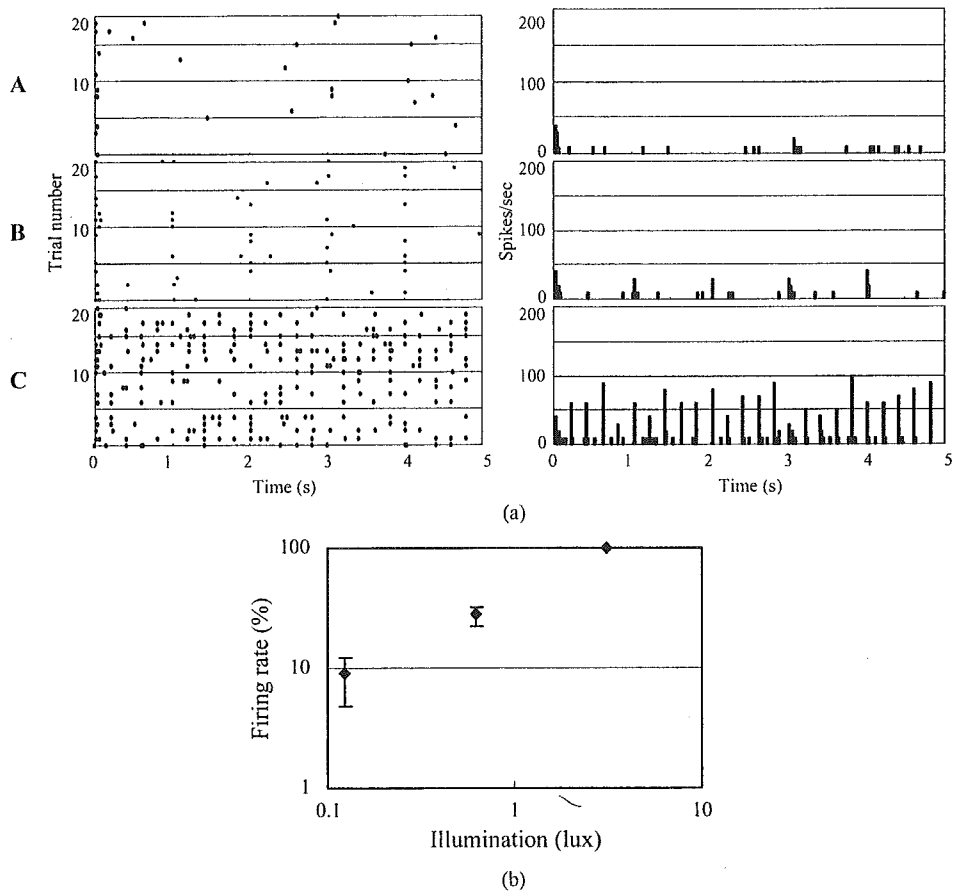

Fig. 7. Experimental results for light-controlled stimulation. (a) Induced response related to infrared light intensity, showing a raster plot (left) and histogram (right; bin width, 5 ms) of the RGC spikes at each intensity (20 trials). (A) 28 μA, 0.2 Hz; (B) 28 μA, 1 Hz; (C) 28 μA, 5 Hz. (b) Experimental results for infrared light-controlled stimulation ($n = 3$).

2.5 mC/cm^2 (Stett et al., 2000), whereas for frog retina, a radius of 100–250 μm has been suggested for charge injection of 1 mC/cm^2 (Li et al., 2005). As frog retinas were employed in the present study, a similar spatial sensitivity distribution can be expected.

Multi-site stimulation is another issue that needs to be evaluated for retinal prostheses. In Pattern electrical stimulation (multi-site stimulation) by a planer electrode array implanted in the eyeball of a blind patient has been reported (Humayun et al., 2003). This stimulation was achieved using a planer electrode array consisting of 16 disc-shaped platinum electrodes in a square 4 × 4 layout, and the device was evaluated in terms of whether testers could distinguish between stimuli patterns. Weiner reported that 1000 or more pixels are required for effective retinal prostheses (Weiner, 2003). However, it remains unknown whether a tester can perceive specific visual sensations as the number of stimulus sites increases. The response of retinal cells to pattern stimulation also remains to be refined. Therefore, the response of the retina to a pattern stimulus must be clarified in detail before clinical trials can proceed.

RGC responses were examined in this study, although the triphasic spikes of the axon responses were also recorded (Fig. 5a). It is considered that the axon responses represent signals transmitted from the RGC response in addition to the response of the axon due to direct stimulation. In the transretinal current stimulation, electric stimuli affect not only RGCs but also other retinal cells (e.g. photoreceptor cells, bipolar cells, amacrine cells, horizontal cells, axons) (Byzov et al., 1968; Toyoda et al., 1977; Kaneko and Saito, 1983; Toyoda and Fujimoto, 1984; Li et al., 2005). Therefore, it is considered that the RGC response recorded in the present experiments consists of two distinct response types; one response reflecting direct excitation of the RGCs by electric stimuli, and another response related to the transmission of responses from other retinal cells to the RGCs. This complex pathway results in inefficient stimulation. Thus, if it were possible to selectively stimulate only non-RGC retinal cells close to the device, more efficient stimulation may be achieved, allowing the power consumption of the stimulus device to be reduced. This is one of the important issues that remains to be addressed in subretinal implantation.

6. Conclusion

The operation of a prototype image sensor was verified through in vitro electrophysiological experiments using a detached frog retina. A new packaging technique was em-

ployed, and the durability of the packaging in a biological environment was confirmed over 16.7 h of testing. The stimulus current output generated by the image sensor was also demonstrated to be sufficient for stimulating the retina. The firing rate was found to be controllable via the stimulus frequency, showing that the PFM photosensor is effective as a retinal prosthesis. Finally, the fabricated image sensor was demonstrated to convert incident light into an electrical stimulus signal that successfully stimulated the retina.

Acknowledgements

The authors thank Prof. Tetsuya Yagi of Osaka University for comments on the in vitro electrophysiological experiments, and Profs. Yasuo Tano and Takashi Fujikado of Osaka University for continuous encouragement. This work was partially supported by the New Energy and Industrial Technology Development Organization (NEDO) of Japan, and Health and Labor Science Research Grants, Japan.

References

Andoh, F., Shimamoto, H., Fujita, Y., 2000. A digital pixel image sensor for real-time readout. IEEE Trans. Elect. Dev. 47 (11), 2123–2127.

Barlett, J.R., Doty, R.W., Lee, B.B., Negrao, N., Overman Jr., W.H., 1977. Deleterious effects of prolonged electrical excitation of striate cortex in macaques. Brain Behav. Evol. 14 (1–2), 46–66.

Brummer, S.B., Turner, M.J., 1977. Electrical considerations for safe electrical stimulation of the nervous system with platinum electrodes. IEEE Trans. Biomed. Eng. 24 (1), 59–63.

Byzov, A.L., Trifonov, Ju.A., 1968. The response to electrical stimulation of horizontal cells in the carp retina. Vision Res. 8 (7), 817–822.

Chow, A.Y., Pardue, M.T., Chow, V.Y., Peyman, G.A., Liang, C., Perlman, J.I., Peachey, N.S., 2001. Implantation of silicon chip microphotodiode arrays into the cat subretinal space. IEEE Trans. Neural Syst. Rehabil. Eng. 9 (1), 86–95.

Deguchi, J., Watanabe, T., Nakamura, T., Nakagawa, Y., Fukushima, T., Jeoung, C.S., Kurino, H., Abe, T., Tamai, M., Koyanagi, M., 2004. Three-dimensionally stacked analog retinal prosthesis chip. Jpn. J. Appl. Phys. 43 (4B), 1685–1689.

Dormer, K.J., 2002. Implantable electronic otologic devices for hearing rehabilitation. In: Finn, W., LoPresti, P. (Eds.), Handbook of Neuroprosthetic Methods. CRC Publishing Company, pp. 237–260.

Eckmiller, R., 1997. Learning retina implants with epiretinal contacts. Ophthalmic Res. 29 (5), 281–289.

Grumet, A.E., Wyatt Jr., J.L., Rizzo 3rd, J.F., 2000. Multi-electrode stimulation and recording in the isolated retina. J. Neurosci. Methods 101 (1), 31–42.

Humayun, M., Propst, R., de Juan Jr., E., McCormil, K., Hickingbotham, D., 1994. Bipolar surface electrical stimulation of the vertebrate retina. Archives of Ophthalmology 112 (1), 110–116.

Humayun, M.S., de Juan Jr., E., Weiland, J.D., Dagnelie, G., Katona, S., Greenberg, R., Suzuki, S., 1999. Pattern electrical stimulation of the human retina. Vision Res. 39 (15), 2569–2576.

Humayun, M.S., Weiland, J.D., Fujii, G.Y., Greenberg, R., Williamson, R., Little, J., Mech, B., Cimmarusti, V., Boemel, G.V., Dagnelie, G., de Juan Jr., E., 2003. Visual perception in a blind subject with a chronic microelectronic retinal prosthesis. Vision Res. 43 (24), 2573–2581.

Ishikane, H., Kawana, A., Tachibana, M., 1999. Short- and long-range synchronous activities in dimming detectors of the frog retina. Visual Neurosci. 16 (6), 1001–1014.

Jensen, R.J., Rizzo 3rd, J.F., Ziv, O.R., Grumet, A., Wyatt, J., 2003. Thresholds for activation of rabbit retinal ganglion cells with an ultrafine, extracellular microelectrode. Invest. Ophth. Vis. Sci. 44 (8), 3533–3543.

Kagawa, K., Isakari, K., Furumiya, T., Uehara, A., Tokuda, T., Ohta, J., Nunoshita, M., 2003. Pixel design of a pulsed CMOS image sensor for retinal prosthesis with digital photosensitivity control. Electron. Lett. 39 (5), 419–421.

Kagawa, K., Yasuoka, K., Ng, D.C., Furumiya, T., Tokuda, T., Ohta, J., Nunoshita, M., 2004. Pulse-domain digital image processing for vision chips employing low-voltage operation in deep-submicrometer technologies. IEEE J. Sel. Top. Quant. 10 (4), 816–828.

Kaneko, A., Saito, T., 1983. Ionic mechanisms underlying the responses of off-center bipolar cells in the carp retina. II. Studies on responses evoked by transretinal current stimulation. J. Gen. Physiol. 81 (4), 603–612.

Li, L., Hayashida, Y., Yagi, T., 2005. Temporal properties of retinal ganglion cell responses to local transretinal current stimuli in the frog retina. Vision Res. 45 (2), 263–273.

Lilly, J.C., Hughes, J.R., Alvord Jr., E.C., Galkin, T.W., 1955. Brief, noninjurious electric waveform for stimulation of the brain. Science 121 (3144), 468–469.

Margalit, E., Maia, M., Weiland, J.D., Greenberg, R.J., Fujii, G.Y., Tores, G., Piyathaisere, D.V., O'Hearn, T.M., Liu, W., Lazzi, G., Dagnelie, G., Scribner, D.A., de Juan Jr., E., Humayun, M.S., 2002. Retinal prosthesis for the blind. Surv. Ophthalmol. 47 (4), 335–356.

Ohta, J., Yoshida, N., Kagawa, K., Nunoshita, M., 2002. Proposal of application of pulsed vision chip for retinal prosthesis. Jpn. J. Appl. Phys. 41 (4B), 2322–2325.

Schanze, T., Wilms, M., Eger, M., Hesse, L., Eckhorn, R., 2002. Activation zones in cat visual cortex evoked by electrical retina stimulation. Graef. Arch. Clin. Exp. 240 (11), 947–954.

Stett, A., Barth, W., Weiss, S., Haemmerle, H., Zrenner, E., 2000. Electrical multisite stimulation of the isolated chicken retina. Vision Res. 40 (13), 1785–1795.

Tehovnik, E.J., 1966. Electrical stimulation of neural tissue to evoke behavioral responses. J. Neurosci. Methods 65 (1), 1–17.

Toyoda, J., Fujimoto, M., Saito, T., 1977. Responses of second-order neurons to photic and electric stimulation of the retina. In: Barlow, H.B., Fatt, P. (Eds.), Vertebrate Photoreception. Academic Press Inc., London, pp. 231–250.

Toyoda, J., Fujimoto, M., 1984. Application of transretinal current stimulation for the study of bipolar-amacrine transmission. J. Gen. Physiol. 84 (6), 915–925.

Weiner, J., 2003. Sight seeing. USC Health Magazine. Available online: http://www.usc.edu/hsc/info/pr/hmm/03winter/sight.html.

Wyatt, J., Rizzo, J.F., 1996. Ocular implants for the blind. IEEE Spectrum 33, 47–53.

Yang, W., 1994. A wide-dynamic-range, low-power photosensor array. In: Proceedings of the IEEE International Solid-State Circuits Conference, pp. 230–231.

Ziegler, D., Linderholm, P., Mazza, M., Ferazzutti, S., Bertrand, D., Ionescu, A.M., Renaud, Ph., 2004. An active microphotodiode array of oscillating pixels for retinal stimulation. Sens. Actuators A 110, 11–17.

Zrenner, E., Stett, A., Weiss, S., Aramant, B.R., Guenther, E., Kohler, K., Miliczek, D.K., Seiler, J.M., Haemmerle, H., 1999. Can subretinal microphotodiodes successfully replace degenerated photoreceptors? Vision Res. 39 (15), 2555–2567.

Zrenner, E., 2002. Will retinal implants restore vision? Science 295 (5557), 1022–1025.

Zrenner, E., Miliczek, K.D., Gabel, V.P., Graf, H.G., Guenther, E., Haemmerle, H., Hoefflinger, B., Kohler, K., Nisch, W., Schubert, M., Stett, A., Weiss, S., 1997. The development of subretinal microphotodiodes for replacement of degenerated photoreceptors. Ophthalmic Res. 29 (5), 269–280.